Available online at www.sciencedirect.com
ScienceDirect
Trans. Nonferrous Met. Soc. China 24(2014) 2034−2040
Transactions of Nonferrous Metals Society of China
www.tnmsc.cn

Crystallographic study of Al_3Zr and Al_3Nb as grain refiners for Al alloys

Feng WANG[1], Dong QIU[1], Zhi-lin LIU[1], John TAYLOR[1], Mark EASTON[2], Ming-xing ZHANG[1]

1. School of Mechanical and Mining Engineering, The University of Queensland, St. Lucia, QLD 4072, Australia;
2. School of Physics and Materials Engineering, Monash University, Clayton, VIC 3800, Australia

Received 17 October 2013; accepted 25 April 2014

Abstract: The potency of Al_3Zr and Al_3Nb as grain refiners for Al alloys was investigated from a crystallographic point of view using the edge-to-edge matching (E2EM) model. The results show that both Al_3Zr and Al_3Nb have small values of interatomic spacing misfit and interplanar spacing mismatch with respect to Al. Furthermore, energetically favourable orientation relationships predicted by the model exist between Al and each of these two intermetallic phases. In the light of the edge-to-edge matching model predictions, it is suggested that both Al_3Zr and Al_3Nb are potent heterogeneous nucleation refiners for Al grains from the crystallographic point of view. The present crystallographic analysis provides a more reasonable explanation for the significant grain refinement obtained in the peritectic Al−Zr and Al−Nb alloys and also provides fresh insight into the understanding of the grain refinement mechanism of Al alloys.

Key words: Al alloy; A_3Zr; Al_3Nb; grain refinement; peritectic; crystallography; E2EM model

1 Introduction

In commercial production, the grain refinement of Al and its alloys through inoculation (i.e., adding master alloys/grain refiners into melt before casting) is common practice to obtain fine, uniform and equiaxed grain structure because fine grains can not only improve the soundness and mechanical properties of castings but also facilitate the subsequent deformation processing and hence ensure consistent performance of the final products [1−4]. Over the past 60 years, extensive research work has been carried out to develop efficient grain refiners for various Al alloys, and many theories/models have been proposed to clarify the mechanism underlying the obtained grain refinement [3−13]. In general, it is agreed that two components, numerous potent nucleants and sufficient effective solutes, are required to achieve effective grain refinement [1−5,9,11,14]. Potent nucleants promote the nucleation of α(Al) at small undercoolings while effective solutes provide constitutional undercooling to trigger further nucleation on adjacent nucleant particles. In spite of the common recognition of these two components, the details of the grain refinement mechanism are still of some controversy as none of the existing theories can fully explain all the observations in both experiments and practice. One of the major controversial and important issues is the determination of key factors that control the efficiency of grain refinement. For instance, a number of new grain refiners [15,16] developed for Mg−Al based alloys and Ti alloys show relatively low grain refining efficiency in comparison with that expected from the combined effect of nucleant particles and solutes. Therefore, it is expected that something important in controlling the grain refinement efficiency is still missing. In addition, it is also noted that the spotlight of the grain refinement of Al alloys is mainly focused on Al−Ti, Al−Ti−B and Al−Ti−C systems since they are the most widely-used grain refiners in the foundry [1,2,11]. However, it has been long realized that many other peritectic Al systems are also associated with appreciable grain refinement of Al such as Al−Zr, Al−Nb and Al−V alloys [17−19]. It is believed that, through the study of these peritectic Al systems, new light may be shed on the factors that control the grain refinement efficiency and hence on the grain refinement mechanism in Al alloys.

Most recently, the grain refining effect of a few peritectic-forming solutes including Zr and Nb on pure Al has been re-examined by WANG et al [20]. Significant grain refinement was obtained by adding Zr and Nb at levels above their maximum solubilities in Al.

Corresponding author: Ming-xing ZHANG; Tel: +61-07-33468709; E-mail: mingxing.zhang@uq.edu.au
DOI: 10.1016/S1003-6326(14)63309-4

Using the *Q*-value model, it is suggested that substantial grain size reduction induced by the addition of Zr and Nb is mainly attributed to the introduction of newly-formed nucleant particles that promote the grain refinement via the enhanced heterogeneous nucleation. Based on the scanning electron microscopy (SEM), energy-dispersive X-ray spectroscopy (EDX), X-ray diffraction (XRD) and thermal analysis results, these in-situ-formed nucleant particles are further identified to be Al_3Zr and Al_3Nb pro-peritectic particles, respectively. Nevertheless, little evidence was provided to confirm the potency of Al_3Zr and Al_3Nb particles as heterogeneous nucleation sites for Al. Therefore, one of the major aims of the this work is to evaluate the nucleation potency of Al_3Zr and Al_3Nb to verify the mechanism proposed in the previous paper.

2 Introduction to edge-to-edge matching model

It is well known that the interfacial energy between the nucleant particle and the metal matrix is of critical significance in determining the potency of nucleant particles [1,2]. In general, good crystallographic matching favours the formation of a low-energy interface between the nucleant particle and the metal matrix, which facilitates the heterogeneous nucleation and hence promotes the grain refinement. Conventionally, the crystallographic matching was simply examined through the calculation of lattice matching based on the lattice parameters [21]. However, in real situations, a great majority of nucleant particles have complex crystal structure, of which crystallographic matching with metal matrix is more than lattice matching because it is the real atoms that form the interface between phases. To overcome the shortcoming of simple calculation of lattice matching, an edge-to-edge matching (E2EM) model was employed.

The edge-to-edge matching model was originally developed by ZHANG and KELLY [22,23] for the examination of actual atomic matching across an interface between adjacent phases of diffusion-controlled phase transformations in solids. It has the ability to predict possible orientation relationship (OR) and the corresponding habit plane/interface with matrix from the first principles. The model is based on a critical assumption that the interfacial crystallographic features are governed by the minimization of the interfacial strain energy through the maximization of atomic matching in the two phases. In general, the atomic row-matching condition can be fulfilled when the atomic rows along the edges of a pair of conjugate crystallographic plane meet at the interface, as shown in Fig. 1 [22,23]. To maximize the atomic matching along the parallel rows, the matching rows should be close packed (CP) or nearly CP directions with small interatomic spacing misfit (f_r). The value of f_r should be less than 10% for a reproducible OR. The matching rows can be either straight or zigzag but the model requires that straight rows match with the straight rows, while zigzag rows match with the zigzag rows. In addition, the conjugate planes containing the matching rows should be a pair of CP or nearly CP planes with similar interplanar spacings. They are termed matching planes. The smaller the interplanar spacing mismatch (f_d<10%) is, the easier the interface meets the row-matching requirement. Once the above conditions are fulfilled, an energetically favourable OR between the two phases can be constructed and expressed in terms of the parallelism of the matching rows and near parallelism of the matching planes. The accuracy of the OR and the orientation of the interface can be further refined by using the Δg parallelism criterion [24,25].

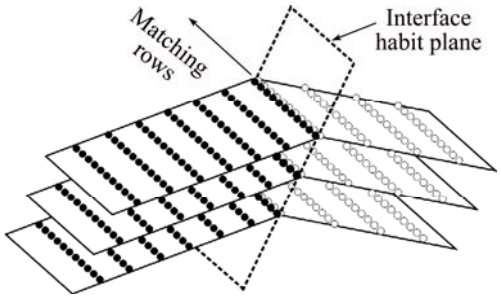

Fig. 1 Schematic diagram of interface meeting edge-to-edge matching conditions [22,23]

In recent years, the E2EM model has been widely applied to the area of grain refinement through the inoculation during solidification. Great success has been achieved in many aspects such as evaluating the potency of grain refiners [26−28], understanding the mechanisms of grain refinement and poisoning phenomena [29−31] and discovering new and effective grain refiners [32] in both Al and Mg alloys. Following the preceding success, in this work, the E2EM model was used to examine the crystallographic matching between the Al matrix and Al_3Zr as well as Al_3Nb particles. As a result, the potency of Al_3Zr and Al_3Nb as nucleant substrates for Al can be evaluated from the crystallographic point of view.

3 Crystallography of Al_3Zr and Al_3Nb with Al matrix

In principle, the E2EM model calculation involves the following two major steps [27,28]: 1) the identification of CP or nearly CP atomic rows and planes of all the phases based on the crystal structure and atomic positions, and 2) the calculation of interatomic misfit, f_r, along the matching rows and the interplanar

spacing mismatch, f_d, between the matching rows based on the corresponding lattice parameters. Table 1 lists the crystal structure, lattice parameters and atomic positions of Al, Al_3Zr and Al_3Nb phases [33]. Using these crystallographic data, the CP or nearly CP atomic rows and planes of these three phases can be identified. As a simple face-centred-cubic (FCC) structure, Al has three possible CP or nearly CP planes: $\{111\}_{Al}$, $\{020\}_{Al}$ and $\{220\}_{Al}$. $\{111\}_{Al}$ is the most CP plane that contains two CP directions: $\langle 110\rangle^{S}_{Al}$ and $\langle 211\rangle^{Z}_{Al}$. For convenience, superscripts of "S" and "Z" are used to distinguish straight and zigzag rows. The second most CP plane, $\{020\}_{Al}$, contains only one CP directions, i.e., $\langle 110\rangle^{S}_{Al}$, while the third most CP plane, $\{220\}_{Al}$, contains two CP directions of $\langle 110\rangle^{S}_{Al}$ and $\langle 211\rangle^{Z}_{Al}$. The Al_3Zr phase has a tetragonal crystal structure with three CP or nearly CP planes. The most CP plane is the $\{401\}_{Al_3Zr}$ plane, which contains three CP rows: $\langle 221\rangle^{Z}_{Al_3Zr}$, $\langle 110\rangle^{S}_{Al_3Zr}$ and $\langle 401\rangle^{S}_{Al_3Zr}$. The second most CP plane of the Al_3Zr phase is the $\{020\}_{Al_3Zr}$ plane that contains only one CP row of $\langle 401\rangle^{S}_{Al_3Zr}$. Another possible CP plane is $\{220\}_{Al_3Zr}$ plane that contains two CP rows of $\langle 221\rangle^{Z}_{Al_3Zr}$ and $\langle 110\rangle^{S}_{Al_3Zr}$. Having a similar structure as Al_3Zr, Al_3Nb also has three CP or nearly CP planes. They are $\{112\}_{Al_3Nb}$, $\{004\}_{Al_3Nb}$, and $\{020\}_{Al_3Nb}$. The $\{112\}_{Al_3Nb}$ plane contains four CP or nearly CP rows that are $\langle 421\rangle^{Z}_{Al_3Nb}$, $\langle 111\rangle^{Z}_{Al_3Nb}$, $\langle 110\rangle^{S}_{Al_3Nb}$, and $\langle 021\rangle^{S}_{Al_3Nb}$, while the $\{004\}_{Al_3Nb}$ contains only one CP row of $\langle 110\rangle^{S}_{Al_3Nb}$. The $\{020\}_{Al_3Nb}$ plane also contains only one CP row of $\langle 021\rangle^{S}_{Al_3Nb}$. The atomic configurations of Al, Al_3Zr and Al_3Nb within their most CP planes are schematically shown in Fig. 2.

Based on the identified CP rows and CP planes, the interatomic spacing misfit along the CP rows between the Al matrix and Al_3Zr as well as Al_3Nb was calculated and listed in Table 2. It is important to note that the interatomic spacing misfit, f_r, is defined by

$$f_r = \frac{|r_M - r_P|}{r_P}, \text{ rather than } \frac{|r_M - r_P|}{r_M} \quad (1)$$

where r_M is the interatomic spacing along a certain CP row of metal matrix, and r_P is the interatomic spacing along the corresponding matching CP row of inoculant particle. It can be seen from Table 2 that all the values of f_r are less than the critical value of 10%. Following that, the interplanar spacing mismatch, f_d, of the CP or nearly CP planes between the Al matrix and Al_3Zr as well as Al_3Nb was further calculated using the equation:

$$f_d = \frac{|d_M - d_P|}{d_P} \quad (2)$$

Table 1 Crystal structure, lattice parameters and atomic positions of Al, Al_3Zr and Al_3Nb phases [33]

Phase	Structure	Space group	Lattice parameter/nm	Atomic position					
				Atom	Multiplicity	Wyckoff letter	x	y	z
Al	Cubic	$Fm\bar{3}m$	a=0.4049	Al	4	a	0	0	0
Al_3Zr	Tetragonal	$I4/mmm$	a=0.4007, c=1.7286	Al	4	c	0	0.5	0
				Al	4	d	0	0.5	0.25
				Al	4	e	0	0	0.361
				Zr	4	e	0	0	0.122
Al_3Nb	Tetragonal	$I4/mmm$	a=0.3841, c=0.8609	Nb	2	a	0	0	0
				Al	2	b	0	0	0.5
				Al	4	d	0	0.5	0.25

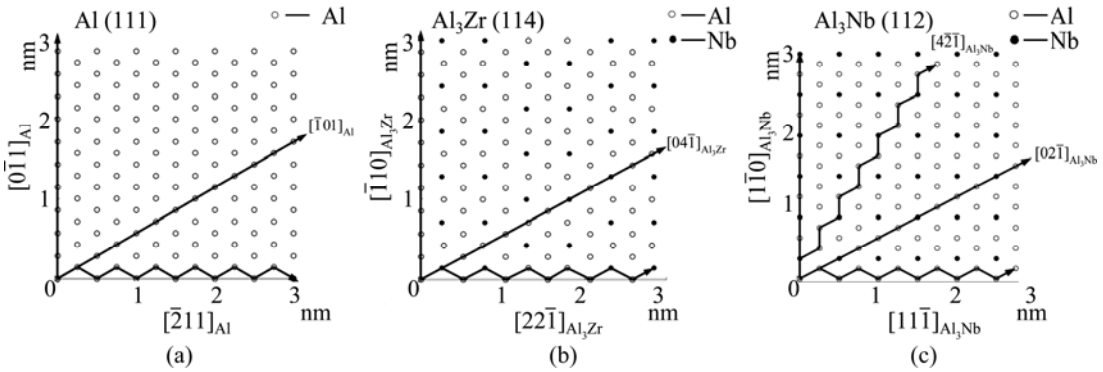

Fig. 2 Atomic configurations of Al (a), Al_3Zr (b) and Al_3Nb (c) on their respective most CP planes (Bold lines highlight CP rows within these planes)

Table 2 Interatomic spacing misfit, f_r, along CP matching rows between Al and Al_3Zr as well as Al_3Nb

Matching plane	f_r/%
$\langle 110\rangle^{S}_{Al} // \langle 110\rangle^{S}_{Al_3Zr}$	1.05
$\langle 110\rangle^{S}_{Al} // \langle 401\rangle^{S}_{Al_3Zr}$	1.99
$\langle 211\rangle^{Z}_{Al} // \langle 221\rangle^{Z}_{Al_3Zr}$	4.03
$\langle 110\rangle^{S}_{Al} // \langle 021\rangle^{S}_{Al_3Nb}$	0.73
$\langle 110\rangle^{S}_{Al} // \langle 110\rangle^{S}_{Al_3Nb}$	5.43
$\langle 211\rangle^{Z}_{Al} // \langle 421\rangle^{Z}_{Al_3Nb}$	3.25
$\langle 211\rangle^{Z}_{Al} // \langle 111\rangle^{Z}_{Al_3Nb}$	2.56

where d_M is the interplanar spacing of a certain CP plane of the metal matrix, and d_P is the interplanar spacing of the corresponding matching CP plane of the inoculant particle. The quantitative results of f_d are graphically illustrated in Fig. 3. As shown in Fig. 3(a), between Al and Al_3Zr, there are only three pairs of CP planes having smaller f_d than 10%. They are $\{111\}_{Al} // \{114\}_{Al_3Zr}$ with f_d=1.34%, $\{020\}_{Al} // \{020\}_{Al_3Zr}$ with f_d=1.05% and $\{220\}_{Al} // \{220\}_{Al_3Zr}$ with f_d=1.05%. Figure 3(b) shows the values of f_d between Al and Al_3Nb. It can be seen that four pairs of CP planes between Al and Al_3Nb have interplanar spacing mismatch, f_d, less than 10%. They are $\{111\}_{Al} // \{112\}_{Al_3Nb}$ with f_d=1.78%, $\{111\}_{Al} // \{004\}_{Al_3Zr}$ with f_d=8.63%, $\{020\}_{Al} // \{004\}_{Al_3Zr}$ with f_d=5.93%, and $\{020\}_{Al} // \{020\}_{Al_3Zr}$ with f_d=5.43%.

According to the E2EM model [27,28], the construction of possible ORs requires that the matching rows must lie in the matching planes. Therefore, the CP row pairs with f_r less than 10% (Table 2) and the corresponding CP planes that contain these row pairs with f_d smaller than 10% (Fig. 3) are represented in Fig. 4. Since a given pair of rows often lie in one or more pair of planes, the arrows are used to indicate the associated plane pairs for a given row pair.

Figure 4(a) shows that, combining the matching row pairs with the plane pairs that contain the matching rows, six possible ORs between Al and Al_3Zr can be obtained. Using the Δg parallelism criterion, these six possible ORs are finally refined to three distinguishable ORs which are listed in Table 3.

Following that, six possible ORs between Al and Al_3Nb are also obtained as shown in Fig. 4(b) by combining the matching row pairs with the plane pairs that carry the matching rows. After the refinement of these six possible ORs, three different ORs are finally predicted as shown in Table 4.

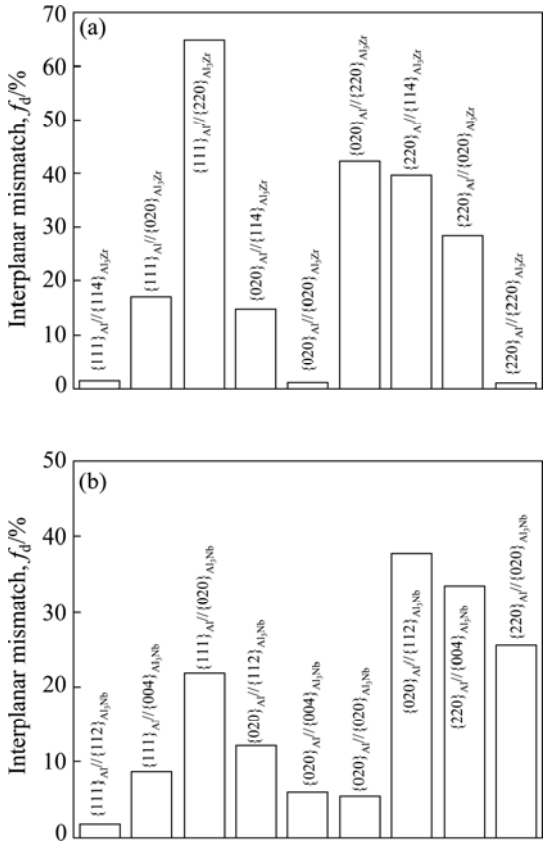

Fig. 3 Interplanar spacing mismatch, f_d, between Al and Al_3Zr (a) and between Al and Al_3Nb (b)

Table 3 Refined crystallographic ORs between Al and Al_3Zr

OR	Nearly parallel direction (1)	Nearly parallel direction (2)	Nearly parallel plane
A1	$[1\bar{1}0]^{S}_{Al_3Zr} // [101]^{S}_{Al}$	$[40\bar{1}]^{S}_{Al_3Zr}$ 1.34° from $[1\bar{1}0]^{S}_{Al}$	$(114)_{Al_3Zr}$ 3.50° from $(11\bar{1})_{Al}$
B1	$[40\bar{1}]^{S}_{Al_3Zr} // [1\bar{1}0]^{S}_{Al}$	$[1\bar{1}0]^{S}_{Al_3Zr}$ 1.26° from $[101]^{S}_{Al}$	$(114)_{Al_3Zr}$ 0.04° from $(11\bar{1})_{Al}$
C1	$[1\bar{1}0]^{S}_{Al_3Zr}$ 0.68° from $[101]^{S}_{Al}$	$[40\bar{1}]^{S}_{Al_3Zr}$ 1.30° from $[1\bar{1}0]^{S}_{Al}$	$(114)_{Al_3Zr}$ 0.68° from $(11\bar{1})_{Al}$

Table 4 Refined crystallographic ORs between Al and Al_3Nb

OR	Nearly parallel direction (1)	Nearly parallel direction (2)	Nearly parallel plane
A2	$[110]^{S}_{Al_3Nb}$ 2.13° from $[0\bar{1}1]^{S}_{Al}$	$[02\bar{1}]^{S}_{Al_3Nb} // [010]^{S}_{Al}$	$(\bar{1}12)_{Al_3Nb}$ 1.07° from $(\bar{1}11)_{Al}$
B2	$[110]^{S}_{Al_3Nb}$ 1.85° from $[0\bar{1}1]^{S}_{Al}$	$[02\bar{1}]^{S}_{Al_3Nb}$ 1.64° from $[010]^{S}_{Al}$	$(\bar{1}12)_{Al_3Nb}$ 1.76° from $(\bar{1}11)_{Al}$
C2	$[110]^{S}_{Al_3Nb} // [0\bar{1}1]^{S}_{Al}$	$[02\bar{1}]^{S}_{Al_3Nb}$ 1.92° from $[010]^{S}_{Al}$	$(\bar{1}12)_{Al_3Nb}$ 0.24° from $(\bar{1}11)_{Al}$

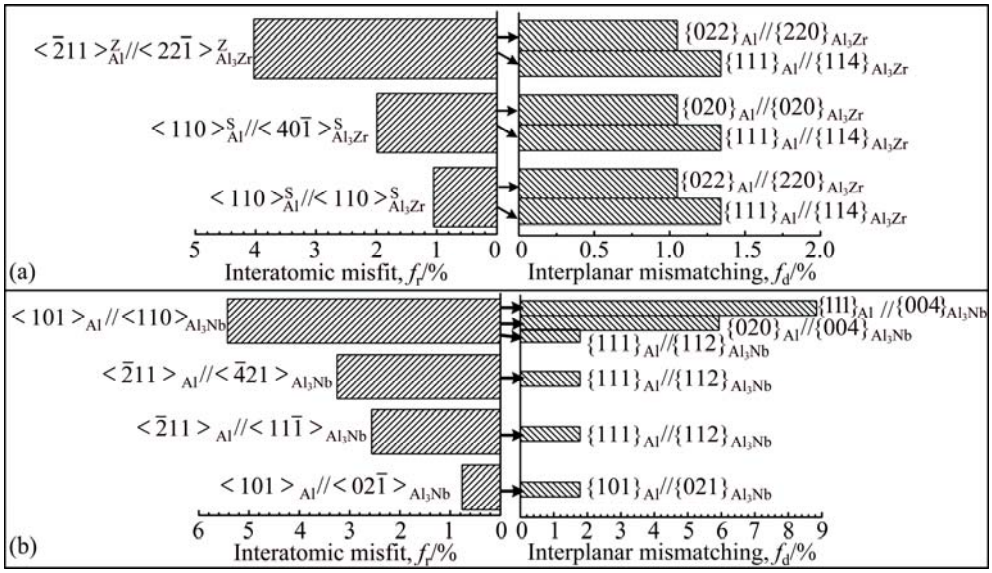

Fig. 4 Graphic representation of matching row pairs (Table 2) and related suitable matching plane pairs (Fig. 3) that carry matching row pairs between Al and Al_3Zr (a), Al and Al_3Nb (b), as predicted by E2EM model

4 Discussion

Based on the above crystallographic analysis using the E2EM model, the potency of Al_3Zr and Al_3Nb as nucleation sites for Al grains can be evaluated. According to the E2EM model, small f_r along the matching rows and low f_d between the matching planes can reduce the interfacial energy between the inoculant particles and metal matrix and hence correspond to high grain refining potency [26−28]. It can be seen from Table 2 and Fig. 3 that both the Al_3Zr and Al_3Nb phases have very small values of f_r and f_d with respect to Al, indicating that these two phases are good grain refiners for Al grains. In particular, the values of f_r and f_d between Al_3Nb and Al are very close to those between Al and Al_3Ti [27] that is one of the most effective grain refiners employed in the industrial practice. This implies that Al_3Nb has the same potential as Al_3Ti as grain refiners for Al grains from the crystallographic point of view.

In the practice of grain refinement by inoculation, it is found that an efficient grain refiner normally has one or more suitable and reproducible OR with the matrix [1,2,11]. Previous studies have proven that the great majority of the reported ORs between the common grain refiners and the Al or Mg matrix are consistent with the predicted ORs by E2EM model [27,28]. It can be seen from Tables 3 and 4 that both the Al_3Zr and Al_3Nb phases have been predicted to have three distinguishable ORs with Al by E2EM model. Unfortunately, unlike the common grain refiners for Al alloys, these predicted ORs between Al and Al_3Zr as well as Al_3Nb cannot be experimentally verified at this stage due to the lack of accurate experimental data on ORs. Currently, the authors are working on the experimental determination of ORs between Al and Al_3Zr as well as Al_3Nb using the electron backscatter diffraction (EBSD) and transmission electron microscopy (TEM). The detailed results will be published in the future papers.

5 Conclusions

1) Both Al_3Zr and Al_3Nb have very small values of interatomic spacing misfit along the matching rows and interplanar spacing mismatch between the matching planes with respect to Al, indicating that these two phases are good nucleant particles for Al grains.

2) Three potential ORs between Al and Al_3Zr are predicted as follows:

OR A1: $[1\bar{1}0]^S_{Al_3Zr}//[101]^S_{Al}$, $[40\bar{1}]^S_{Al_3Zr}$ 1.34° from $[1\bar{1}0]^S_{Al}$, $(114)_{Al_3Zr}$ 3.50° from $(11\bar{1})_{Al}$;

OR B1: $[40\bar{1}]^S_{Al_3Zr}//[1\bar{1}0]^S_{Al}$, $[1\bar{1}0]^S_{Al_3Zr}$ 1.26° from $[101]^S_{Al}$, $(114)_{Al_3Zr}$ 0.04° from $(11\bar{1})_{Al}$;

OR C1: $[1\bar{1}0]^S_{Al_3Zr}$ 0.68° from $[101]^S_{Al}$, $[40\bar{1}]^S_{Al_3Zr}$ 1.30° from $[1\bar{1}0]^S_{Al}$, $(114)_{Al_3Zr}$ 0.68° from $(11\bar{1})_{Al}$.

Three distinguishable ORs between Al and Al_3Nb were predicted as follows:

OR A2: $[110]^S_{Al_3Zr}$ 2.13° from $[0\bar{1}1]^S_{Al}$, $[02\bar{1}]^S_{Al_3Nb}//[101]^S_{Al}$, $(\bar{1}12)_{Al_3Nb}$ 1.07° from $(\bar{1}11)_{Al}$;

OR B2: $[110]^S_{Al_3Nb}$ 1.85° from $[0\bar{1}1]^S_{Al}$, $[02\bar{1}]^S_{Al_3Nb}$ 1.64° from $[101]^S_{Al}$, $(\bar{1}12)_{Al_3Nb}$ 1.76° from $(\bar{1}11)_{Al}$;

OR C2: $[110]^{S}_{Al_3Nb} // [0\bar{1}1]^{S}_{Al}$, $[02\bar{1}]^{S}_{Al_3Nb}$ 1.92° from $[101]^{S}_{Al}$, $(\bar{1}12)_{Al_3Nb}$ 0.24° from $(\bar{1}11)_{Al}$.

Acknowledgement

The authors are very grateful to the Australian Research Council for funding support. Feng WANG would also like to acknowledge the support of China Scholarship Council.

References

[1] MURTY B S, KORI S A, CHAKRABORTY M. Grain refinement of aluminium and its alloys by heterogeneous nucleation and alloying [J]. International Materials Reviews, 2002, 47: 3−29.

[2] QUESTED T E. Understanding mechanisms of grain refinement of aluminium alloys by inoculation [J]. Materials Science and Technology, 2004, 20: 1357−1369.

[3] EASTON M A, STJOHN D H. Grain refinement of aluminum alloys: Part I. The nucleant and solute paradigms—A review of the literature [J]. Metallurgical and Materials Transactions A, 1999, 30: 1613−1623.

[4] EASTON M A, STJOHN D H. Grain refinement of aluminum alloys: Part II. Confirmation of, and a mechanism for, the solute paradigm [J]. Metallurgical and Materials Transactions A, 1999, 30: 1625−1633.

[5] CIBULA A. The grain refinement of aluminium alloy castings by additions of titanium and boron [J]. Journal of the Institute of Metals, 1951, 80: 1−16.

[6] MARCANTONIO J A, MONDOLFO L F. Grain refinement in aluminum alloyed with titanium and boron [J]. Metallurgical Transactions, 1971, 2: 465−471.

[7] BACKERUD L, SHAO Y. Grain refining mechanisms in aluminium as a result of additions of titanium and boron (I) [J]. Aluminium, 1991, 67: 780−785. (in Germany)

[8] BACKERUD L, JOHNSSON M, GUSTAFSON P. Grain refining mechanisms in aluminium as a result of additions of titanium and boron (II) [J]. Aluminium, 1991, 67: 910−915. (in Germany)

[9] JOHNSSON M, BACKERUD L, SIGWORTH G K. Study of the mechanism of grain refinement of aluminum after additions of Ti- and B-containing master alloys [J]. Metallurgical Transactions A: Physical Metallurgy and Materials Science, 1993, 24: 481−491.

[10] MOHANTY P S, GRUZLESKI J E. Mechanism of grain refinement in aluminium [J]. Acta Metallurgica et Materialia, 1995, 43: 2001−2012.

[11] GREER A L, COOPER P S, MEREDITH M W, SCHNEIDER W, SCHUMACHER P, SPITTLE J A. Grain refinement of aluminium alloys by inoculation [J]. Advanced Engineering Materials, 2003, 5: 81−91.

[12] QUESTED T E, GREER A L. Grain refinement of Al alloys: Mechanisms determining as-cast grain size in directional solidification [J]. Acta Materialia, 2005, 53: 4643−4653.

[13] StJOHN D H, QIAN M, EASTON M A, CAO P. The Interdependence Theory: The relationship between grain formation and nucleant selection [J]. Acta Materialia, 2011, 59: 4907−4921.

[14] JOHNSSON M, BACKERUD L. The influence of composition on equiaxed crystal growth mechanisms and grain size in Al alloys [J]. Zeitschrift fur Metallkunde, 1996, 87: 216−220.

[15] BERMINGHAM M J, MCDONALD S D, DARGUSCH M S, StJOHN D H. Grain-refinement mechanisms in titanium alloys [J]. Journal of Materials Research, 2008, 23: 97−104.

[16] StJOHN D H, QIAN M, EASTON M A, CAO P, HILDEBRAND Z. Grain refinement of magnesium alloys [J]. Metallurgical and Materials Transactions A, 2005, 36: 1669−1679.

[17] EBORALL M D. Grain refinement of aluminium and its alloys by small additions of other elements [J]. Journal of the Institute of Metals, 1949, 76: 295−320.

[18] MARCANTONIO J A, MONDOLFO L F. Nucleation of aluminium by several intermetallic compounds [J]. Journal of the Institute of Metals, 1970, 98: 23−27.

[19] CROSSLEY F A, MONDOLFO L F. Mechanism of grain refinement in aluminum alloys [J]. Transactions of the American Institute of Mining and Metallurgical Engineers, 1951, 191: 1143−1148.

[20] WANG F, LIU Z L, QIU D, TAYLOR J A, EASTON M A, ZHANG M X. Revisiting the role of peritectics in grain refinement of Al alloys [J]. Acta Materialia, 2013, 61: 360−370.

[21] BRAMFITT B. The effect of carbide and nitride additions on the heterogeneous nucleation behavior of liquid iron [J]. Metallurgical Transactions, 1970, 1: 1987−1995.

[22] ZHANG M X, KELLY P M. Edge-to-edge matching and its applications: Part I. Application to the simple HCP/BCC system [J]. Acta Materialia, 2005, 53: 1073−1084.

[23] ZHANG M X, KELLY P M. Edge-to-edge matching and its applications: Part II. Application to Mg−Al, Mg−Y and Mg−Mn alloys [J]. Acta Materialia, 2005, 53: 1085−1096.

[24] ZHANG W Z, PURDY G R. O-lattice analyses of interfacial misfit. I: General considerations [J]. Philosophical Magazine A, 1993, 68: 279−290.

[25] ZHANG W Z, YE F, ZHANG C, QI Y, FANG H S. Unified rationalization of the Pitsch and T–H orientation relationships between Widmanstätten cementite and austenite [J]. Acta Materialia, 2000, 48: 2209−2219.

[26] QIU D, ZHANG M X, FU H M, KELLY P M, TAYLOR J A. Crystallography of recently developed grain refiners for Mg−Al alloys [J]. Philosophical Magazine Letters, 2007, 87: 505−514.

[27] ZHANG M X, KELLY P M, EASTON M A, TAYLOR J A. Crystallographic study of grain refinement in aluminum alloys using the edge-to-edge matching model [J]. Acta Materialia, 2005, 53: 1427−1438.

[28] ZHANG M X, KELLY P M, QIAN M, TAYLOR J A. Crystallography of grain refinement in Mg−Al based alloys [J]. Acta Materialia, 2005, 53: 3261−3270.

[29] QIU D, TAYLOR J A, ZHANG M X. Understanding the co-poisoning effect of Zr and Ti on the grain refinement of cast aluminum alloys [J]. Metallurgical and Materials Transactions A, 2010, 41: 3412−3421.

[30] QIU D, TAYLOR J A, ZHANG M X, KELLY P M. A mechanism for the poisoning effect of silicon on the grain refinement of Al−Si alloys [J]. Acta Materialia, 2007, 55: 1447−1456.

[31] QIU D, ZHANG M X, TAYLOR J A, FU H M, KELLY P M. A novel approach to the mechanism for the grain refining effect of melt superheating of Mg−Al alloys [J]. Acta Materialia, 2007, 55: 1863−1871.

[32] QIU D, ZHANG M-X, TAYLOR J A, KELLY P M. A new approach to designing a grain refiner for Mg casting alloys and its use in Mg−Y-based alloys [J]. Acta Materialia, 2009, 57: 3052−3059.

[33] DAAMS J L, VILLARS P, VUCHT J H V. Atlas of crystal structure types for intermetallic phases [M]. Ohio: ASM International, 1991: 4146−4149.

Al_3Zr 和 Al_3Nb 作为铝合金晶粒细化剂的晶体学研究

汪 锋[1]，邱 冬[1]，刘峙麟[1]，John TAYLOR[1]，Mark EASTON[2]，张明星[1]

1. School of Mechanical and Mining Engineering, The University of Queensland, St. Lucia, QLD 4072, Australia;
2. School of Physics and Materials Engineering, Monash University, Clayton, VIC 3800, Australia

摘　要：利用 edge-to-edge matching 模型从晶体学角度研究 Al_3Zr 和 Al_3Nb 两种金属间化合物作为铝合金晶粒细化剂的有效性。结果表明，Al_3Zr 和 Al_3Nb 两种金属间化合物和铝之间的原子间距错配和面间距错配值都很小。此外，模型预测 Al_3Zr 和 Al_3Nb 两种金属间化合物与铝之间存在良好的晶粒取向关系。根据模型理论可以从晶体学角度证明这两种金属间化合物对铝合金是有效的晶粒异质形核细化剂。本晶体学研究为包晶铝合金 Al−Zr 和 Al−Nb 中出现的明显晶粒细化现象提供了合理解释，同时为理解晶粒细化机理提供了新方法。

关键词：铝合金；Al_3Zr；Al_3Nb；晶粒细化；包晶；晶体学；E2EM 模型

(Edited by Wei-ping CHEN)